Nonthermal nature of photo-induced insulator-to-metal transition in NbO2

Rana, R.; Klopf, J. M.; Grenzer, J.; Schneider, H.; Helm, M.; Pashkin, A.;

Originally published:

January 2019

Physical Review B 99(2019)4, 041102(R)

DOI: https://doi.org/10.1103/PhysRevB.99.041102

Non-thermal nature of photo-induced insulator-to-metal transition in NbO_2

Rakesh Rana[1*], J. Michael Klopf[2], Jörg Grenzer[1], Harald Schneider[1], Manfred Helm[1,3], and Alexej Pashkin[1**]

[1]*Institute of Ion Beam Physics and Material Research, Helmholtz-Zentrum-Dresden-Rossendorf, 01328 Dresden, Germany*

[2]*Institute of Radiation Physics, Helmholtz-Zentrum Dresden-Rossendorf, 01328 Dresden, Germany*

[3]*Institute of Applied Physics, Technische Universität Dresden, 01062 Dresden, Germany*

Abstract:

We study the photo-induced metallization process in niobium dioxide NbO_2. This compound undergoes the thermal insulator-to-metal transition at the remarkably high temperature of 1080 K. Our optical pump – terahertz probe measurements reveal the ultrafast switching of the film on a sub-picosecond timescale and the formation of a metastable metallic phase when the incident pump fluence exceeds the threshold of ~10 mJ/cm^2. Remarkably, this threshold value corresponds to the deposited energy which is capable of heating NbO_2 only up to 790 K, thus, evidencing the non-thermal character of the photo-induced insulator-to-metal transition. We also observe an enhanced formation of the metallic phase above the second threshold of ~17.5 mJ/cm^2 which corresponds to the onset of the thermal switching. The transient optical conductivity in the metastable phase can be modeled using the Drude-Smith model confirming its metallic character. The present observation of non-thermal transition evidences a leading role played by electronic correlations in NbO_2 and can serve as an important test bed for understanding photo-induced phenomena in strongly correlated oxides.

[*]r.rana@hzdr.de

[**]a.pashkin@hzdr.de

Understanding the subtleties of the insulator-to-metal transition (IMT) in strongly correlated oxides is an important challenge in condensed matter physics. One of the prime examples is the IMT at 340 K in VO_2 which is a $3d^1$ transition-metal oxide. The orbital-assisted collaborative effort of Mott physics and a Peierls transition is suggested as the IMT mechanism [1, 2]. Ultrafast time-resolved studies have demonstrated the photo-induced switching of VO_2 from the insulating phase into a metastable metallic state on a sub-100 fs time scale when the incident pump fluence exceeds a certain threshold value [3, 4]. While the ultrafast photoemission data [5] show evidence for a purely electronic character of the metallization immediately after the photoexcitation, it is known that the long-living metallic phase can be induced only when the absorbed pump energy exceeds the threshold necessary to heat the sample above T_c [6]. Thus, the enthalpy change in the lattice subsystem across the photo-induced phase transition may play an important role in the formation of the metastable metallic phase. On the other hand, the results of other terahertz - [7] and electron diffraction [8] studies of VO_2 indicate that in a certain range of pump fluences, the metallization can be induced without the structural transition into the high-temperature rutile phase. A better understanding of this complex ultrafast switching behavior calls for a search for related oxide systems where the photo-induced metallization can be clearly identified as a non-thermal phase transition.

NbO_2 is a $4d^1$ system isovalent with VO_2 which undergoes an IMT at the transition temperature T_c = 1080 K [9,10]. This phase transition is accompanied by a transformation from a regular rutile structure ($P4_2/mnm$) having two formula units per unit cell in the metallic phase above T_c to a distorted rutile structure $I4_1/a$ with 32 formula units per unit cell for the insulating phase below T_c as illustrated in Fig. 1 [11,12]. This fact is related to a stronger bond existing between local Nb dimers due to a better overlap of 4d orbitals causing larger orbital splitting between $d_{\|}$ (occupied) states and the e^{π}_{g} (unoccupied) states, thus ensuring a robust Peierls effect in the insulating phase [13,14]. The formation of Nb dimers in the insulating phase has a quasi-one-dimensional character along the c-axis and is attributed to the instability due softening of the phonon mode at the *P*-wavevector, $q_p = \left(\frac{1}{4}, \frac{1}{4}, \frac{1}{2}\right)$ [10]. However, the exact nature of the phase transition is still debated. Using density functional theory (DFT) it was speculated that the dimerization alone rather than electron correlations is responsible for the opening of the band gap [15]. Recent DFT and cluster-dynamical mean-field theory calculations stressed the role of electronic correlations which are also relevant for NbO_2, (although to a lesser extent than in VO_2) and thus should be taken into account along

with the Peierls distortion, for a complete description in the insulating phase [16]. NbO_2 serves as an ideal choice for understanding the IMT in VO_2 as there are a few interesting similarities: both belong to the d^1 family of compounds and the (V-V or Nb-Nb) dimers in the insulating phase exhibit tilting with respect to the rutile c-axis [17]. Furthermore, in the high-temperature rutile phase, VO_2 and NbO_2 crystals have nearly the same axial ratio of c/a = 0.625. This value becomes slightly larger for monoclinic VO_2 and smaller for the tetragonal NbO_2, however, the two structures seem to be nearly degenerate near the phase transition [17]. Recently the ultrafast switching of NbO_2 films on femtosecond time scale has been demonstrated and compared with the response of VO_2 films using near-infrared pump-probe measurements [18].

Here we present a time-resolved optical pump– terahertz (THz) probe (OPTP) spectroscopic study of a NbO_2 thin film and demonstrate that the metastable metallic phase can be induced for pump fluences which heat the system to temperatures far below T_c. Our results identify a large range of pump fluences between 10 and 17.5 mJ/cm^2 over which a purely non-thermal metallization can be achieved.

The 190 nm thick epitaxial NbO_2 film was grown on (111) $MgAl_2O_4$ substrate using pulsed laser deposition technique [19,20]. Time-resolved measurements were performed using a femtosecond Ti:sapphire regenerative amplifier operating at a 1 kHz repetition rate and the central wavelength of ~ 800 nm (1.55 eV). The measured penetration depth at the pump wavelength for our NbO_2 film is 60 nm.

The sample was excited using the optical pump with the photon energy of 1.55 eV which is well above the direct (1.3 eV) and indirect (0.7 eV) band gaps of NbO_2 [15,20]. This process leads to the creation of a large number of non-equilibrium free carriers and a strong increase of optical conductivity at THz frequencies. As a result, the THz transmission through the thin film demonstrates a drop which is roughly proportional to the concentration of the free carriers. The dynamics of this process can be monitored from the temporal evolution of the differential THz transmission $\Delta T/T$. We found no significant phase shift in $\Delta T/T$. Therefore, the maximum change in THz conductivity $\Delta\sigma_1$ is proportional to $|\Delta T/T|$ and it can be easily estimated based on the thin-film approximation. The dependence of $\Delta\sigma_1$ on the pump-probe delay time t is shown in Fig. 2. Around zero delay time the pump-probe signal experiences an initial steep rise on the timescale limited only by the temporal resolution of our OPTP setup [19]. For low pump fluences, it is followed by the fast relaxation within 1 ps and the recovery of the initial insulating state. This behavior is similar to the behavior of VO_2 described in

previous studies and it is usually assigned to the recombination (localization) of the photoexcited charge carriers [4,7,21]. We find that as the fluence is increased above 10 mJ/cm^2, $\Delta\sigma_1$ does not vanish after the initial relaxation and remains finite even after tens of picoseconds (see figure 2(a) and the inset). This remanence of $\Delta\sigma_1$ suggests the formation of metastable metallic domains [21]. The measured values of $\Delta\sigma_1$ can be directly compared to the dc conductivity reported in the literature by Sakata, et al., [22]. The dc conductivity of NbO_2 in the metallic phase (around 1200 K) is about 600-700 $(\Omega cm)^{-1}$ [22]. This value is approximately 5-6 times higher than the measured THz conductivity averaged within the photoexcited layer. Such ratio is also typical for VO_2 thin films and was reported, for example, by Hilton et al. [21] and Kübler et al. [4]. The reason for the lower conductivity in the photo-induced phase is related to the inhomogeneous metallization character. The complete photo-induced switching is practically unreachable in thin films even in the heat diffusion regime due to the presence of a substrate which serves as a heat sink and maintains nearly constant temperature at the film's boundary.

To gain further insight into the relaxation mechanism, the $\Delta\sigma_1$ was fitted with a biexponential fitting function, $\boldsymbol{A_f}\exp(-t/\boldsymbol{\tau_f}) + \boldsymbol{A_s}\exp(-t/\boldsymbol{\tau_s}) + \sigma_{1offset}$, where $\boldsymbol{\tau_f}$ (A_f) and $\boldsymbol{\tau_s}$ ($\boldsymbol{A_s}$) represent the time constant (and amplitude) of the fast and the slow processes, respectively and $\sigma_{1offset}$ describes the constant offset. The latter value $\sigma_{1offset}$ represents a long-lived photo-induced metallic response. In figure 3 (a), the value of $\sigma_{1offset}$ exhibits a distinctive dependence on pump fluence with a typical dual threshold behavior. To capture this, extrapolation of the linear fits to the values of $\sigma_{1offset}$ in this plot gives two characteristic threshold fluences: Φ_{T1} ~ 10 mJ/cm^2 and Φ_{T2} ~ 17.5 mJ/cm^2. Above Φ_{T1}, the non-vanishing $\sigma_{1offset}$ starts to increase moderately, and above Φ_{T2} the slope becomes steeper with a rapid increase. It is noteworthy that the value of the first threshold fluence Φ_{T1} for NbO_2 is nearly twice the corresponding value observed for VO_2 [4,6]. For NbO_2 the contribution from constant A_f capturing the amplitude of the fast dynamics increases linearly as a function of pump fluence which is consistent with a semiconducting-type response as seen in figure 3 (c). On the other hand, the amplitude of the slow relaxation $\boldsymbol{A_s}$ shows a sublinear increase so that the ratio $\boldsymbol{A_f}/\boldsymbol{A_s}$ increases from 4 to 10 from the lowest to highest pump fluence.

In analogy with Ref. [23], the slower dynamics captured by $\boldsymbol{\tau_s}$ is interpreted as the thermalization of high energy phonons heated by the recombination of the photoexcited charge carriers. Here we rely on the fact that VO_2 (and similarly NbO_2) may be treated as a molecular crystal of strongly correlated dimers [2,4]. As depicted in Fig. 3(b), the slow

relaxation shows a decrease from 6 ps and saturates to a value of 3 ps above Φ_{T1}. The faster dynamics described by $\tau_f \approx 0.4$ ps is close to the temporal resolution of our OPTP setup and can be assumed independent on the pump fluence.

As discussed earlier the effective thickness of our NbO_2 film for the pump excitation was found to be ~ 60 nm for the wavelength of ~ 800nm. Estimating the effective pump pulse energy deposited, a pump fluence of 1 mJ/cm^2 corresponds to an enthalpy change of ~ 3.52 kJ/mol in the case of NbO_2 [22]. Knowing this we can compare the temperature (***T****) of the photoexcited NbO_2 layer immediately after pumping with previously reported equilibrium enthalpy changes [22]. The enthalpy difference between the room temperature insulating phase of NbO_2 and its metallic phase at 1080 K is about 62.4 kJ/mol including the transition latent heat of 3.4 kJ/mol [24]. The threshold fluences Φ_{T1}, Φ_{T2} and the upper limit of measured fluence (24.7mJ/cm^2) correspond to ***T**** - values of 790 K, 1080 K, and 1390 K in the photoexcited layer, respectively (figure 3(a)). The first threshold Φ_{T1} nearly corresponds to the energy of 33 kJ/mol for the NbO_2. The second threshold Φ_{T2} corresponds to the T_c where ***T**** starts to exceed Tc and a part of the thin film may be switched also thermally. Naturally, the activation of the additional switching mechanism leads to the more rapid growth of the metallic phase fraction within the insulating phase and is well captured in figure 3(a) by a rapidly increasing $\sigma_{1offset}$ above a fluence of Φ_{T2}. In order to check the purely nonthermal IMT the excitation regime between Φ_{T1} and Φ_{T2} (790 K < ***T**** < 1080K) is most appropriate. This is because the final temperature of the surface layer (***T****) is well below T_c and the metastable metallic phase must be driven by the non-thermal action of the pump pulse.

To confirm the metallic character of the photo-induced phase in NbO_2 we present in figure 4(a-b) the transient THz conductivity $\Delta\sigma(\omega)$, for pump fluences of 15 mJ/cm^2 (***T**** ~ *960 K*) and 20.8 mJ/cm^2 (***T**** ~ *1210 K)*. The finite conductivity response for 15 mJ/cm^2 is shown in figure 4(a), and attests its purely nonthermal character below T_c. To provide a physical description of the carrier properties, the transient complex conductivity $\Delta\sigma(\omega)$ of the NbO_2 film can be fitted using the Drude-Smith model given by, $\Delta\sigma(\omega) = \frac{\varepsilon_o \omega_p^2 \tau_o}{1-i\omega\tau_o}\left(1 + \frac{c}{1-i\omega\tau_o}\right)$, wherein ε_o, ω_p, and τ_o represents the vacuum permittivity, the plasma frequency, and the carrier scattering time, respectively [25]. This model presents a good description of the ultrafast photo-induced IMT in several systems where there is a coexistence of metallic and insulating nanodomains [26, 27]. Here the fitting parameter ***c*** which is attributed to the persistence of the velocity after first scattering event can have values between -1 and 0, while the former value indicates full backscattering and/or carrier localization while the latter

corresponds to the Drude model. Recently, an elaborated extension of the Drude-Smith formula with physically meaningful parameters has been developed [28].

The electron localization in the metallic domains and the nonzero value of $\boldsymbol{c}$ points towards backscattering at the domain walls or grain boundaries, which are revealed in our film by x-ray diffraction [19]. During the ultrafast phase transition, electrons are excited into the conduction band which results in the formation of the metallic domains in the insulating matrix. A mutual phase competition between the insulating and the metallic nano-domains will occur. The overall macroscopic character of the film is dictated by the growth and coalescence of the insulating or metallic domains. For NbO_2 the value of *c* varies from -0.52 to -0.65 as the fluence is increased from 15 mJ/cm^2 to 20.8 mJ/cm^2 suggesting a more Drude-like character for the former than for the latter (see Table I). This fact is rather surprising owing to the fact that the metallic domains increase in size at the higher fluence evidenced by the conductivity increase. However, the electronic temperature also becomes higher. As a result, the electron velocity in the photoexcited state increases and the ratio of the metallic domain size to the mean free path may decrease, even if the metallic domains slightly expand, leading to a stronger localization of the charge transport [7, 29]. Nevertheless, owing to relatively large errors in determination of $\boldsymbol{c}$ in the present study (see Table I), a detailed analysis of the localization effects is not possible and demands a separate investigation.

We find that $\Delta\sigma(\omega)$ decreases as a function of pump probe delay time (see Fig. 2) which suggests that domains of the insulating phase grow and coalesce at the expense of metallic domains. The carrier concentration was calculated using $N = \varepsilon_o m^* \omega_p^2 / e^2$, where the effective mass $m^*=12.7m_o$ [9], m_o is the electron mass and the dc conductivity is computed using $\sigma_o = \varepsilon_o \tau_o \omega_p^2 (1 + c)$. Our calculated values of *N* are of the order of (10^{19} cm^{-3}) lesser than the value of *N* (~10^{22} cm^{-3}) [9] when the sample is thermally heated above T_c. This is expected as we switch only 60nm depth of the film. However, there is only a marginal increase in the value of *N* with pump fluence from 15 mJ/cm^2 to 20.8 mJ/cm^2, which suggests the effect of the matrix of insulating NbO_2 in capturing the photoexcited electrons via recombination limiting the overall conductivity and metallicity. The mobility was found using $\mu = q\tau_o(1 + c)/m^*$ and the values for a 1 ps probe delay were 2.7 cm^2/Vs for 15 mJ/cm^2 which increases to 2.9 cm^2/Vs for 20.8 mJ/cm^2. These values are moderately higher than the value of 0.5 cm^2/Vs reported for a crystalline NbO_2 sample at 600 K [9].

We now discuss the OPTP results on the NbO_2 film for longer probe delays and the observed non-thermal character of the photo-induced metallic state. In NbO_2 samples we do not find

$\Delta\sigma_1$ to increase with the delay time for several tens of ps, even for maximum fluence 24.7 mJ/cm^2 [figure 2(a)], which is in contrast to VO_2 where a slow increase in the magnitude of $\Delta\sigma_1$ is often noted above threshold excitation at later delays [7,21]. This increase indicates that for our NbO_2 film the metallicity remains restricted to the region of the penetration depth of 60 nm in the NbO_2 film and beyond this thickness, deeper layers remain insulating. Consequently, this effect is also seen in the $\Delta\sigma(\omega)$, which exhibits only a marginal decrease between the measurement at a 1 ps probe delay and at a 2.5 ps delay as shown in figure 4(b) and Table I. Cocker et al. reported a similar effect in VO_2 at low temperatures [7]. In the case of VO_2, the ultrafast phase transition possesses an intermediate step with the formation of a monoclinic metallic state [5, 8]. The photo-doping of the holes in the 3d valence band causes an instantaneous collapse of the band gap without structural modification [5] confirming the triggering role of the Mott mechanism in the IMT [1, 2]. On the other hand, the weaker Coulomb correlation for 4*d* electrons and an enhanced Peierls instability discovered by recent theoretical modelling [15] indicate that the hierarchy of the Mott and Peierls mechanisms may be reversed in the case of NbO_2. Nevertheless, the presented results demonstrate that the photo-induced metallic state can be achieved even when the deposited energy is smaller than the enthalpy barrier to the high-temperature rutile structure of NbO_2. This would not be possible in a standard (pure) Peierls insulator where the IMT necessarily implies a complete structural transformation. Thus, electronic correlation effects must play a certain role in the formation of the insulating state that can be clarified in course of further experiments.

In conclusion, we demonstrate the non-thermal nature of the ultrafast insulator-to-metal transition in epitaxial NbO_2 thin film and confirm the metallic character of the photo-induced phase by transient THz conductivity measurements. The high T_c of NbO_2 results in a large range over which the ultrafast intermediate metallic phase can be decoupled from the thermally driven structural transition. These results indicate that NbO_2 represents an important test bed for an understanding of the photo-induced IMT in strongly correlated oxides. In particular, further time-resolved studies using structural probes such as x-ray or electron diffraction may provide important clues about the interplay of electronic and structural degrees of freedom in this interesting case of the purely non-thermal phase transition.

References:

1. M. W. Haverkort, Z. Hu, A. Tanaka, W. Reichelt, S. V. Streltsov, M. A. Korotin, V. I. Anisimov, H. H. Hsieh, H.-J. Lin, C. T. Chen, D. I. Khomskii, and L. H. Tjeng, Phys. Rev. Lett. **95**, 196404 (2005)
2. S. Biermann, A. Poteryaev, A. I. Lichtenstein, and A. Georges, Phys. Rev. Lett. **94**, 026404 (2005)
3. S. Wall, D. Wegkamp, L. Foglia, K. Appavoo, J. Nag, R.F. Haglund Jr, J. Stähler, and M. Wolf, Nat. Commun. **3**, 721 (2012)
4. C. Kübler, H. Ehrke, R. Huber, R. Lopez, A. Halabica, R. F. Haglund, Jr., and A. Leitenstorfer, Phys. Rev. Lett. **99**, 116401 (2007)
5. D. Wegkamp, M. Herzog, L. Xian, M. Gatti, P. Cudazzo, C. L. McGahan, R. E. Marvel, R. F. Haglund, Jr., A. Rubio, M. Wolf, and J. Stähler, Phys. Rev. Lett. **113**, 216401 (2014)
6. A. Pashkin, C. Kübler, H. Ehrke, R. Lopez, A. Halabica, R. F. Haglund, Jr., R. Huber, and A. Leitenstorfer, Phys. Rev. B **83**, 195120 (2011)
7. T. L. Cocker, L. V. Titova, S. Fourmaux, G. Holloway, H.-C. Bandulet, D. Brassard, J.-C. Kieffer, M. A. El Khakani, and F. A. Hegmann, Phys. Rev. B **85**, 155120 (2012)
8. V. R. Morrison, R. P. Chatelain, K. L. Tiwari, A. Hendaoui, A. Bruhács, M. Chaker, and B. J. Siwick, Science **346**, 445–448 (2014)
9. Y. Sakai, N. Tsuda, and T. Sakata, J. Phys. Soc. Jpn. **54**, 1514 (1985)
10. R. Pynn, J. D. Axe, and R. Thomas, Phys. Rev. B **13**, 2965 (1976)
11. A. A. Bolzan, C. Fong, B. J. Kennedy, and C. J. Howard, J. Solid State Chem. **113**, 9 (1994)
12. K. Momma and F. Izumi, J. Appl. Crystallogr. **44**, 1272-1276 (2011)
13. J. B. Goodenough, Phys. Rev. **117**, 1442 (1960)
14. V. Eyert, Europhys. Lett. **58**, 851 (2002)
15. A. O'Hara and A. A. Demkov, Phys. Rev. B **91**, 094305 (2015).
16. W. H. Brito, M. C. O. Aguiar, K. Haule, and G. Kotliar, Phys. Rev. B **96**, 195102 (2017)
17. Z. Hiroi, Prog. Solid State Chem. **43**, 47 (2015)
18. M. R. Beebe, J. M. Klopf, Y. Wang, S. Kittiwatanakul, J. Lu, S. A. Wolf, and R. A. Lukaszew, Opt. Mater. Express **7**, 213 (2017)
19. See Supplemental Material at …..for the X-ray and Raman characterization of the NbO_2 thin film, the description of the OPTP setup and the modelling of the temperature profile.
20. F. J. Wong, N. Hong, and S. Ramanathan, Phys. Rev. B **90**, 115135 (2014)
21. D. J. Hilton, R. P. Prasankumar, S. Fourmaux, A. Cavalleri, D. Brassard, M. A. El Khakani, J. C. Kieffer, A. J. Taylor, and R. D. Averitt, Phys. Rev. Lett. **99**, 226401 (2007)
22. T. Sakata, K. Sakata, G. Höfer, and T. Horiuchi, J. Cryst. Growth **12**, 88 (1972)
23. M. Mitrano, G. Cotugno, S. R. Clark, R. Singla, S. Kaiser, J. Stähler, R. Beyer, M. Dressel, L. Baldassarre, D. Nicoletti, A. Perucchi, T. Hasegawa, H. Okamoto, D. Jaksch, and A. Cavalleri, Phys. Rev. Lett. 112, 117801 (2014)

24. K. T. Jacob, C. Shekhar, and M. Vinay, J. Chem. Eng. Data **55**, 4854 (2010)
25. N. V. Smith, Phys. Rev. B **64**, 155106 (2001)
26. M. Walther, D. G. Cooke, C. Sherstan, M. Hajar, M. R. Freeman, and F. A. Hegmann, Phys. Rev. B **76**, 125408, (2007)
27. P. U. Jepsen, B. M. Fischer, A. Thoman, H. Helm, J. Y. Suh, R. Lopez, and R. F. Haglund, Jr., Phys. Rev. B **74**, 205103 (2006)
28. T. L. Cocker, D. Baillie, M. Buruma, L. V. Titova, R. D. Sydora, F. Marsiglio, and F. A. Hegmann, Phys. Rev. B **96**, 205439 (2017)
29. H. Němec, P. Kužel, and V. Sundström, Phys. Rev. B **79**, 115309 (2009)

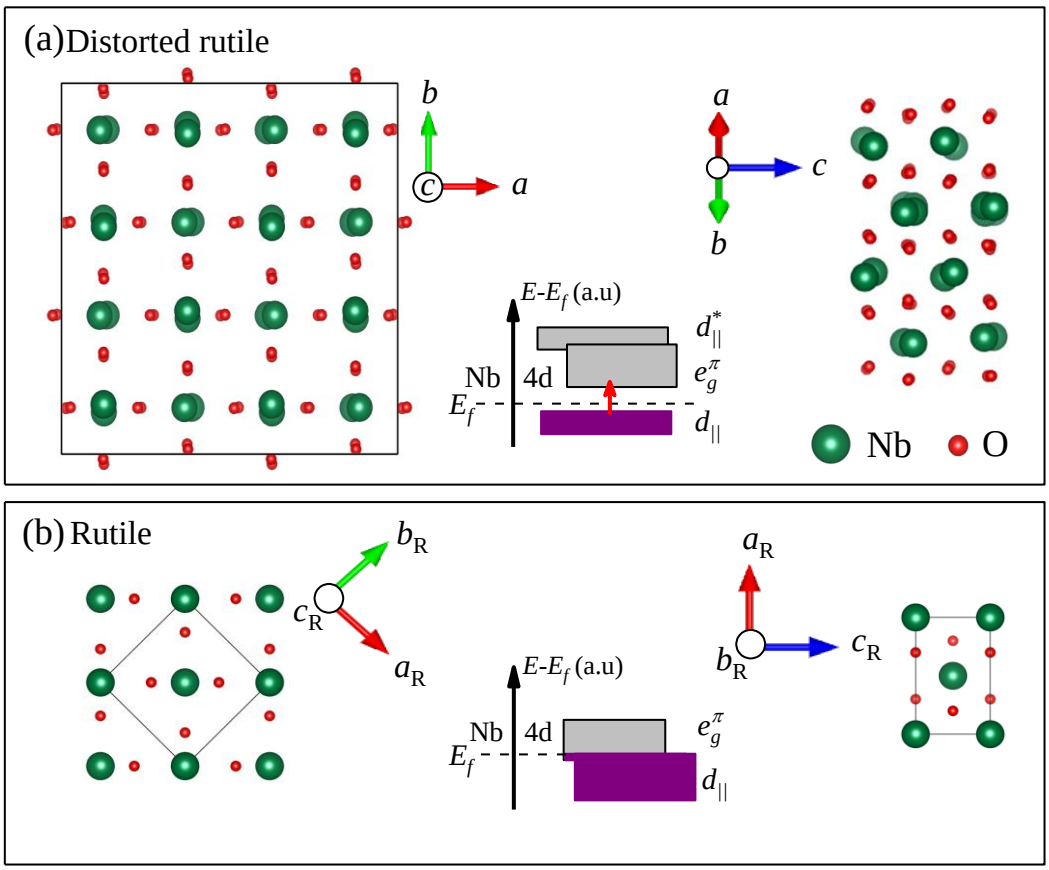

Fig. 1. Crystal structure of NbO_2 in (a) body centered tetragonal (*bct*) distorted rutile structure below the insulator-metal transition temperature (T_c) and (b) rutile structure above T_c [11,12]. In the middle of each panel a schematic band structure for the respective phase is depicted [18]. The vertical red arrow in the top panel band structure illustrates the photo-excitation by the pump pulse with the photon energy of 1.55 eV.

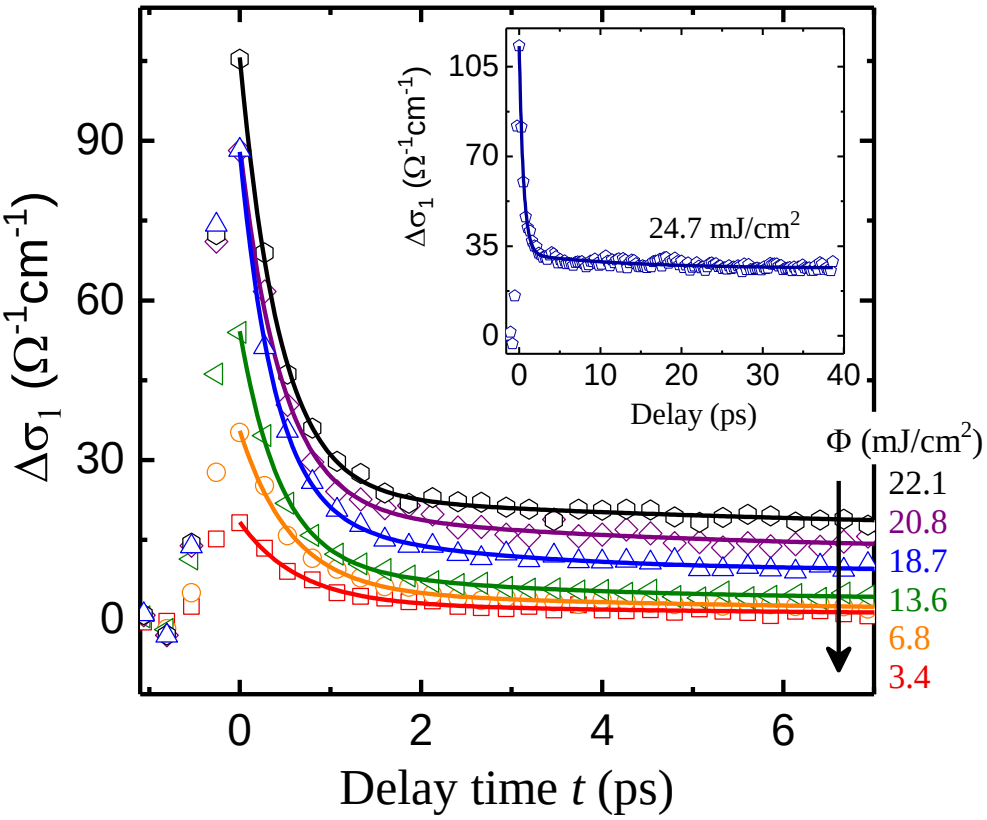

Fig. 2. Spectrally integrated transient change of the THz conductivity $\Delta\sigma_1$ as a function of the pump-probe delay time t for selected fluences at a substrate temperature of 295 K. The inset depicts a signal at longer delay times. The experimental data are fitted with bi-exponential functions.

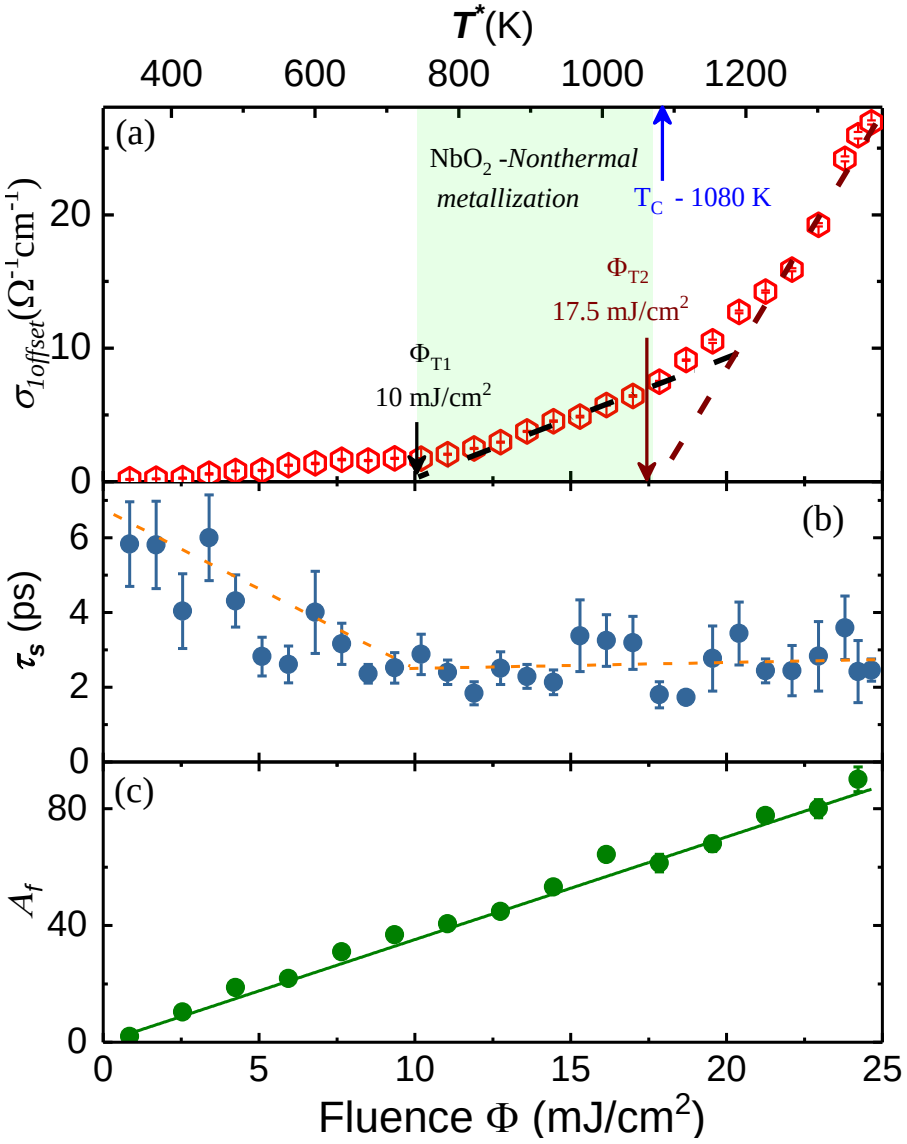

Fig. 3. (a) $\sigma_{1offset}$ as a function of the pump fluence. The dashed lines show the linear extrapolations that give two characteristic threshold fluences Φ_{T1} and Φ_{T2}, here $\boldsymbol{T^*}$ denotes the temperature of the photoexcited NbO_2 layer immediately after the pumping. (b) The slow relaxation time $\boldsymbol{\tau_s}$ as a function of fluence (orange dash line is a guide to the eye). (c) The amplitude of the fast relaxation $\boldsymbol{A_f}$ as a function of fluence (straight green line is a linear fit).

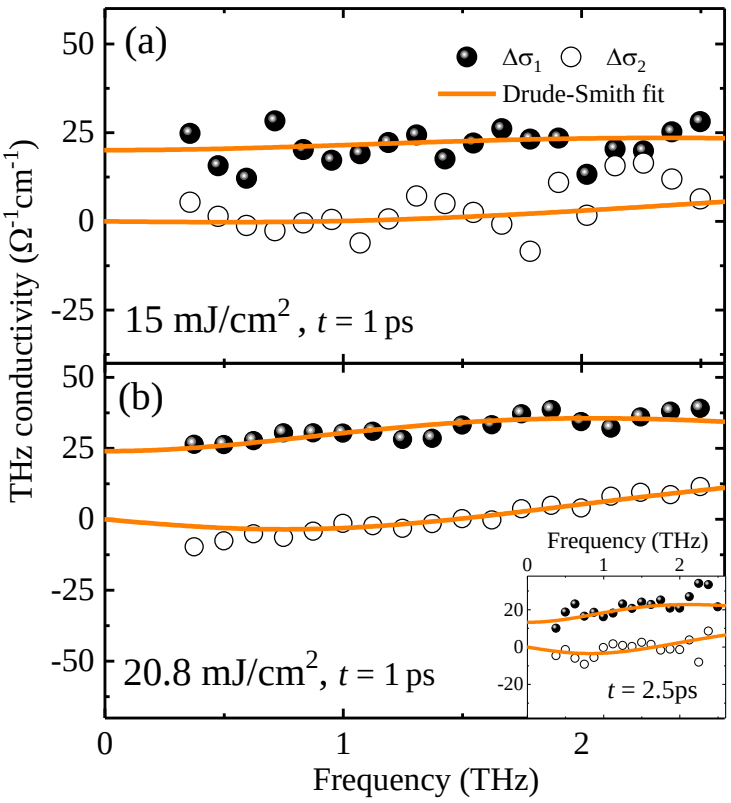

Fig. 4. (a) The transient THz complex conductivity spectra where $\Delta\sigma_1$ is the real and $\Delta\sigma_2$ is the imaginary part of the transient complex conductivity for pump probe delays (t) after photoexcitation. Here solid lines represent fits using the Drude-Smith model.

Table I. The Drude-Smith fitting parameters obtained after fitting the transient optical conductivity data.

Fluence	**Delay time (ps)**	ω_p **(THz)**	τ_o **(fs)**	c	N $(*10^{19}\ cm^{-3})$	σ_o $(\Omega^{-1}cm^{-1})$
15 mJ/cm^2	1	107	41±13	-0.52±0.06	4.6	20
20.8 mJ/cm^2	1	115	60±10	-0.65±0.02	5.3	25
20.8 mJ/cm^2	2.5	90	58±12	-0.62±0.04	3.2	16